ACS APPLIED MATERIALS & INTERFACES

Research Article

www.acsami.org

Easy Fabrication of Macroporous Gold Films Using Graphene Sheets as a Template

Shengtong Sun and Peiyi Wu*

State Key Laboratory of Molecular Engineering of Polymers, Department of Macromolecular Science, and Laboratory of Advanced Materials, Fudan University, Shanghai 200433, People's Republic of China

Supporting Information

ABSTRACT: We demonstrate a facile new and environmentally friendly strategy to fabricate monolithic macroporous gold (MPG) films using graphene sheets as a sacrificial template. Gold nanoparticle (AuNP) decorated graphene sheets were prepared by a one-pot simultaneous reduction of graphene oxide (GO) and gold precursor ($HAuCl_4$) by sodium citrate. Two thermal annealing methods, direct thermal annealing in air and a two-step thermal treatment (in N_2 first and subsequently in air), were then employed to remove the template (graphene sheets), which can both produce macroporous structures, but with distinctly different morphologies. We additionally investigated the porosity evolution mechanism as well as the effect of graphene/Au weight ratio and annealing temperature on the nanoarchitecture. The two-step treatment has a more significant templating effect than direct thermal annealing to fabricate MPG films because of the existence of a preaggregation process of AuNPs assisted by graphene sheets in N_2. Moreover, the resulting MPG films were found to exhibit excellent surface-enhanced Raman scattering (SERS) activity. Our method can be hopefully extended to the synthesis of other porous materials (such as Ag, Cu, Pt, and ceramic) and much wider applications.

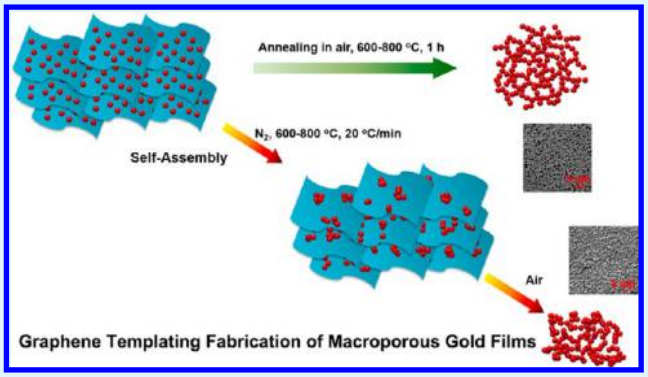

KEYWORDS: *macroporous gold, graphene, gold nanoparticles, templating, thermal annealing, surface-enhanced Raman scattering*

1. INTRODUCTION

Porous metals represent a new class of functional materials combining properties of metals such as good thermal and electrical conductivity, catalytic activity, and ductility with properties characteristic of nanoarchitectures such as aerogels with high surface area, low density and high strength-to-weight ratio.[1−3] Owing to a rich surface chemistry, porous metals are of great interests in catalysis,[4−6] electrocatalysis,[7,8] sensing,[9] supercapacitor,[10] optical[11] and biological[12,13] applications. Currently, the most common strategies to make porous metals are mainly based on dealloying,[14,15] combustion,[3,16] templating,[17−19] sol−gel assembly,[20] electrochemical etching[21] and laser ablation.[22] Among them, templating is a rather powerful method to incorporate and control porosity within metals by using sacrificial inorganic or organic materials as templates, which, however, is usually limited in practice by the difficult infiltration of metal or metal precursors into templates (often colloidal nanospheres).[3]

Graphene is regarded as one of the most promising building blocks to make various functional composite materials due to its excellent mechanical, thermal, and electrical properties.[23,24] Benefiting from the unique 2D planar nanocarbon structure, graphene is proved to be an excellent substrate for immobilizing metal nanoparticles.[25−27] Plenty of reports show that the metal nanoparticles anchored on graphene sheets potentially exhibit enhanced catalytic, electrical and optical activities. For example, gold nanoparticle/graphene oxide (AuNP/GO) composites prepared by noncovalent attachment of AuNPs premodified with 2-mercaptopyridine to GO sheets exhibit significantly higher catalytic activities than the corresponding AuNPs in the reduction of *o*-nitroaniline to 1,2-benzenediamine by $NaBH_4$.[28] By electrostatic self-assembly and thermal annealing, the resultant AuNP embedded graphene films show improved electrical and thermal conductivity as well as electrochemical performance.[29,30] By combination of metallic nanostructures and graphene, a drastic Raman enhancement and efficient adsorption of aromatic molecules can also be observed, which are suitably used as surface-enhanced Raman scattering (SERS) substrates.[26−28]

Although nearly all the previous reports up to now about graphene and metallic nanoparticles are related to the preparation and properties of their composites, in this paper, we prefer to remove the graphene sheets from their composites by a simple thermal annealing process. We found that monolithic macroporous gold (MPG) films can also be easily fabricated by this method. Herein, graphene sheets are found to be a new kind of sacrificial template except commonly used colloidal nanospheres and organic soft templates. The

Received: February 25, 2013
Accepted: March 22, 2013
Published: March 22, 2013

operation conditions are easy and environmentally friendly without using any toxic or corrosive reagents, and the porosity and morphology of MPG films can be finely controlled by adjusting the graphene/Au weight ratio and operation conditions. Additionally, the evolution mechanism of porosity and their SERS activity are also explored.

2. EXPERIMENTAL SECTION

2.1. Preparation of GO Sheets. GO was prepared by a modified Hummers' method.[31] Briefly, expandable graphite powders (5 g, 8000 mesh, Aladdin Co. Ltd.) and sodium nitrate (2.5 g) were mixed in concentrated H_2SO_4 (115 mL) at 0 °C, followed by the addition of potassium permanganate (15 g) under vigorous stirring. After increasing the temperature to 35 °C, excess deionized water (300 mL) was added to the mixture before stirring for another 30 min and the temperature was then increased to 90 °C for 15 min before adding 30% H_2O_2 (100 mL). The resultant suspension was filtered, washed with 5% HCl and dialyzed for 7 days to remove the remaining metal species. The GO aqueous dispersion was diluted prior to use.

2.2. Preparation of Graphene/Au Composites. Graphene/Au composites were prepared by a simple one-pot method according to our previous paper.[32] $HAuCl_4{\cdot}3H_2O$ (0.6, 1.6, 2.5, or 6.5 mM), GO (0.1 mg/mL) and sodium citrate (10 mg/mL) were mixed with the assistance of sonication for 2 min and then placed in an oil bath at 100 °C for 24 h with stirring. After washing by centrifugation until the supernatant was colorless, the resultant graphene/Au composites (G/Au = 1:1.3, 1:3.1, 1:5.0 and 1:6.3, named by the feed ratio due to the complete reduction reaction) were redispersed in water (graphene, 0.1 mg/mL).

2.3. Preparation of Graphene/Au Hybrid Papers and MPG Films through Thermal Annealing. Graphene/Au hybrid papers were prepared by vacuum-assisted filtration of 20 mL graphene/Au composite aqueous dispersions with Millipore filter membrane (φ50 mm*0.2 μm, mixed cellulose ester). The hybrid paper was then washed with water and air-dried.

Two annealing methods were adopted to prepare MPG films:

(a) Direct thermal annealing: the dried graphene/Au hybrid papers were placed in a preheated furnace and annealed at 600−800 °C in air for 1 h.

(b) Two-step thermal annealing: the dried graphene/Au hybrid papers were placed in a sealed chamber equipped for thermogravimetric analysis (TGA) measurement and heated to 600−800 °C in N_2 atmosphere at a heating rate of 20 °C/min. Then the hybrid papers were exposed in air by opening the chamber immediately to obtain yellow MPG films. For the control experiment, after heating to 600 °C, the sample was cooled down to room temperature still in N_2 atmosphere.

2.4. Characterization. The ultraviolet−visible (UV−vis) spectra of graphene/Au aqueous dispersions (graphene, 0.01 mg/mL) were measured on a Hitachi U-2910 spectrophotometer. High-resolution transmission electron microscopy (HRTEM) images were taken with a JEOL JEM 2011 at 200 kV. TGA was performed under N_2 or air atmosphere with a Perkin-Elmer Thermal Analyzer at a heating rate of 20 °C/min. Scanning electron microscopy (SEM) images were recorded on a TS 5136MM scanning electron microscope. Energy dispersive X-ray (EDX) analysis was performed on a Hitachi S-4800 field-emission scanning electron microscope (FE-SEM). The MPG samples for SERS experiments were immersed in the aqueous solution of Nile bule A (NBA) with a specified concentration (10^{-4}, 10^{-5} and 10^{-6} M) for 12 h and air-dried before Raman measurements. Raman spectra were recorded on a Renishaw inVia Reflex micro-Raman spectrometer with 785 nm laser excitation. A 200× objective was used to focus the laser beam and to collect the Raman signals. To ensure the obtained spectra were comparable, the settings, including the laser's power and the exposure time, were all the same.

3. RESULTS AND DISCUSSION

AuNPs decorated graphene sheets with increasing weight ratios (G/Au = 1:1.3, 1:3.1, 1:5.0, 1:6.3) were synthesized by a one-pot simultaneous reduction of GO and gold precursor ($HAuCl_4$) by sodium citrate as described in our previous paper.[32] The resulting graphene/Au composites can be well dispersed in water showing two apparent absorption peaks in UV−vis spectra at 255 nm (restored $\pi-\pi$ conjugated structure of graphene) and 533 nm (plasmonic peak of AuNPs) (Figure S1 in Supporting Information). From TEM images (Figure S2) the AuNPs are uniformly attached to the graphene sheets with an average size of 20 nm. TGA curves (Figure S3) exhibit a gradual content increase of AuNPs in resultant composites as the initial feed ratio changes.

Graphene/Au hybrid papers were then prepared by a commonly used vacuum-assisted filtration method[29] and subsequently air-dried. To choose a proper annealing temperature, we perform TGA measurements of graphene/Au hybrid film (G/Au = 1:3.1) under air atmosphere, as shown in Figure 1. Graphene/Au hybrid film shows the maximum decomposition peak around 400 °C, corresponding to the complete removal of graphene sheets from their composites. Thus an annealing temperature above 500 °C should be necessary for the fabrication of MPG films. In this paper, we mainly chose 600 and 800 °C as the annealing temperatures for comparison.

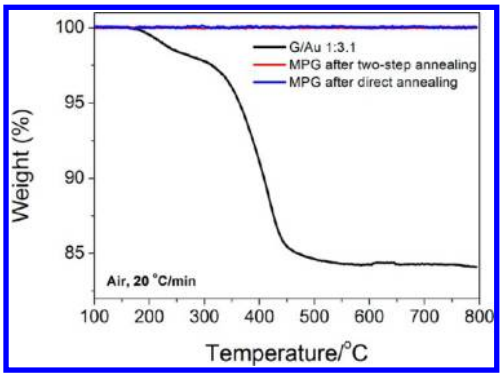

Figure 1. TGA curves of the graphene/Au hydrid film (G/Au = 1:3.1) and the obtained MPG films after two-step annealing and direct annealing under an air atmosphere.

Two thermal annealing methods were employed: (a) anneal graphene/Au hybrid papers at 600−800 °C in air for 1 h to directly remove the template (graphene sheets); (b) heat graphene/Au hybrid papers to 600−800 °C in N_2 atmosphere (20 °C/min) first and then expose the hybrid papers immediately in air to remove the template (graphene sheets). The SEM images of the exterior of MPG films upon two thermal annealing procedures at an annealing temperature of 600 °C are shown in Figure 2. The color of graphene/Au hybrid paper changes from black to yellow after annealing, suggesting the removal of graphene components. The removal of graphene components can also be evidenced by the TGA curves of the resultant MPG films under air atmosphere. As shown in Figure 1, nearly no weight loss can be observed for the two MPG films up to 800 °C, indicating that the graphene sheets have been largely removed through combustion in air.

It is noted that both the two methods can produce MPG films, but with apparently different morphologies. By direct annealing in air, the uniform and compact graphene/Au multilayer films would transform into MPG films with

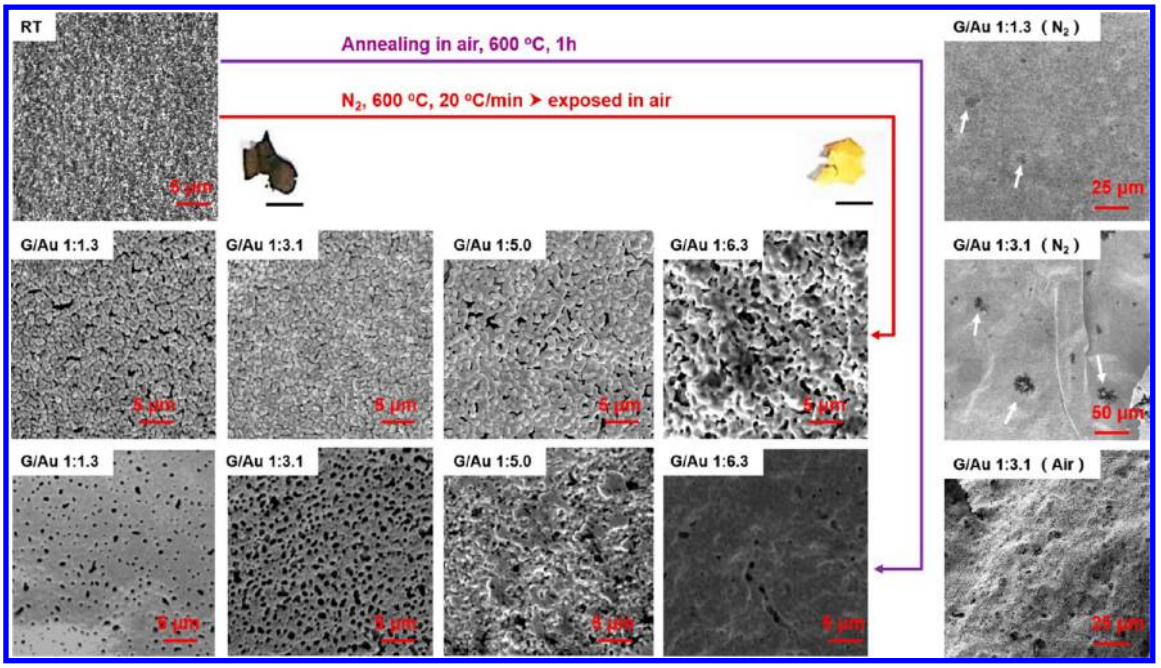

Figure 2. SEM images of the exterior of MPG films upon two thermal annealing procedures (annealing temperature = 600 °C) produced from initial graphene/Au hybrid papers with different weight ratios. The right three images are of smaller magnification, showing the porous structure is large-scalely uniform. The white arrows mark the positions of shaded areas. The scale bar under the images of the two pieces represents 50 mm.

completely interconnected networks, while by a two-step treatment (annealing in N_2 and then exposing in air) openly bicontinuous MPG films with recognizable ligaments and pores can be obtained. The formation of bicontinuous porous structure by the two-step annealing treatment can also be confirmed by TEM (Figure S4). Additionally, take the samples G/Au =1.1.3 and 1:3.1 for example, the porous structures formed by the two annealing methods are both uniform on a large scale, as presented in Figure 2. However, for comparison, applying the two annealing methods to the films formed by the deposition of only AuNPs on Si substrates leads to merely messily distributed porous structures (Figure S5), indicating the significant templating effect of graphene sheets.

Except for the annealing treatment method, different graphene/Au weight ratios also result in different morphologies and porosity, as shown in Figure 2. For direct annealing in air, only the samples with lower content of AuNPs (G/Au = 1:1.3, 1:3.1) exhibit defined interconnected porous structures, while there are only minor amounts of pores on the surface of the samples with higher content of AuNPs (G/Au = 1:5.0, 1:6.3). The sample G/Au = 1:3.1 with moderate content of AuNPs has the highest porosity. For the two-step annealing treatment, all the four samples show an openly bicontinuous structure with large ligaments and small pores. We also plotted the pore and ligament size distributions according to the SEM images in Figure 2, which can be found in Figure S6 in the Supporting Information, and all the average pore and ligament sizes have been listed in Table 1. Generally, increasing the content of AuNPs in graphene/Au composites leads to an obvious increase of both the pore and ligament sizes in the resultant MPG films. Judging from the morphology and porosity evolution of porous structures, it is supposed that the two annealing treatment methods may adopt distinctly different mechanisms.

The annealing temperature also affects the porosity and morphology of the resultant MPG films. As shown in Figure 3,

Table 1. Average Pore and Ligament Sizes of MPG Films Obtained from Different Annealing Methods, G/Au Ratios, and Annealing Temperatures

	two-step annealing				direct annealing	
	600 °C		800 °C		600 °C	800 °C
G/Au	pore (nm)	ligament (nm)	pore (nm)	ligament (nm)	pore (nm)	pore (nm)
1:1.3	330	610			460	
1:3.1	250	620	390	820	580	2330
1:5.0	350	730				
1:6.3	550	1080				

either two-step or direct annealing at 400 °C cannot produce any porous nanostructures, in conformity with our former analysis that an annealing temperature above 500 °C should be necessary for the fabrication of MPG films. Increasing the annealing temperature to 800 °C leads to the formation of well-defined porous structures for both the two annealing methods, similar to those in Figure 2 at the annealing temperature of 600 °C. The pore and ligament size distribution plots of the MPG films upon annealing at 800 °C can be found in Figure S7 in the Supporting Information, and the average sizes are also presented in Table 1. It is noted that a higher annealing temperature would cause the increase of both the pore and/or ligament sizes, either for two-step annealing or for direct annealing, indicating that during thermal annealing there may exist a very similar change between AuNPs for the two annealing methods.

Before the discussion of porosity evolution mechanism, we also find that there are several shaded areas on the surfaces of the samples after the two-step treatment, as indicated by the arrows in Figure 2. More evidence for the shaded areas can be found in Figure 4. It seems to be some crystalline residues after the removal of graphene sheets in air. We performed the EDX analysis of the sample G/Au = 1:3.1 before and after the two-

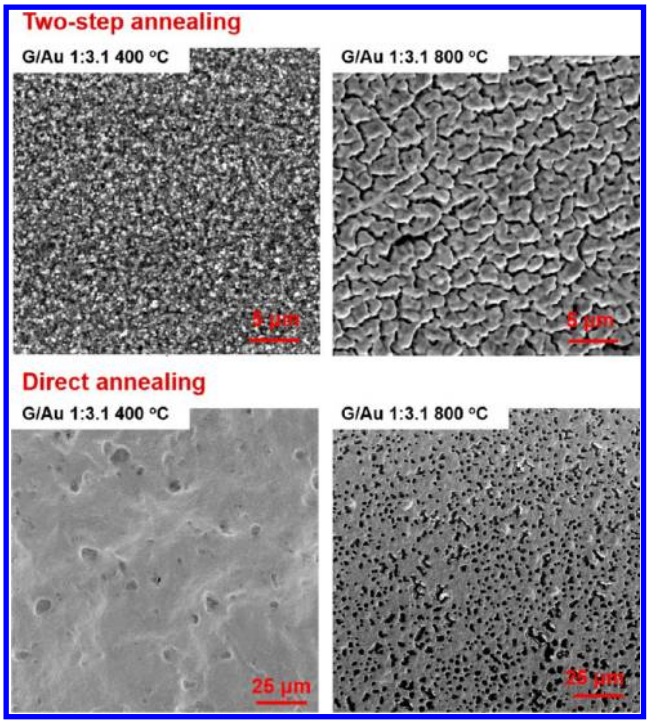

Figure 3. SEM images of the exterior of the sample G/Au = 1:3.1 upon two-step annealing and direct annealing at 400 and 800 °C.

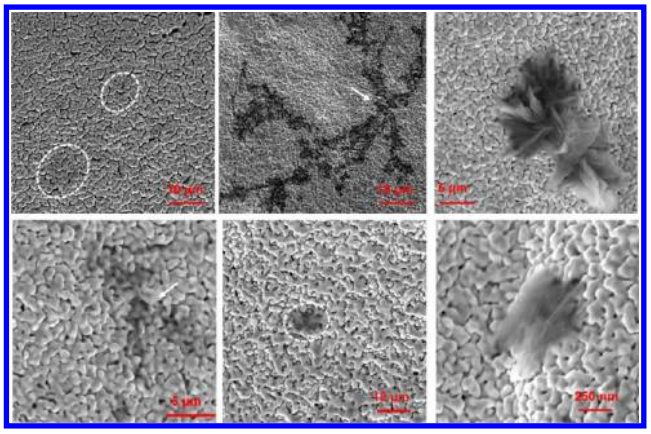

Figure 4. Evidence for the shaded areas in MPG films (G/Au = 1:3.1).

step annealing treatment with/without the shaded area, as shown in Figure 5. The element Na should come from the sodium citrate moieties attached on the surface of graphene sheets and AuNPs as a capping agent.[33] The element C content changes strongly support the removal of graphene sheets and the formation of MPG. The existence of small amounts of C in the resultant MPG film may arise from the incomplete combustion during the two-step annealing treatment because of a drastic temperature drop after exposing the film in air. It is worth noting that the shaded area has a much higher content of Na, which reveals that it may be the residual decomposition product of sodium citrate moieties (such as Na_2O). Obviously, upon thermal annealing in N_2 at 600 °C, all the surface oxygen groups on graphene sheets and AuNPs start to decompose,[34] which inevitably leads to the detachment of AuNPs from graphene sheets. It is presumed that the uncapped AuNPs would tend to aggregate and fuse into larger AuNPs at the high temperature, similar to the thermal coarsening of nanoporous

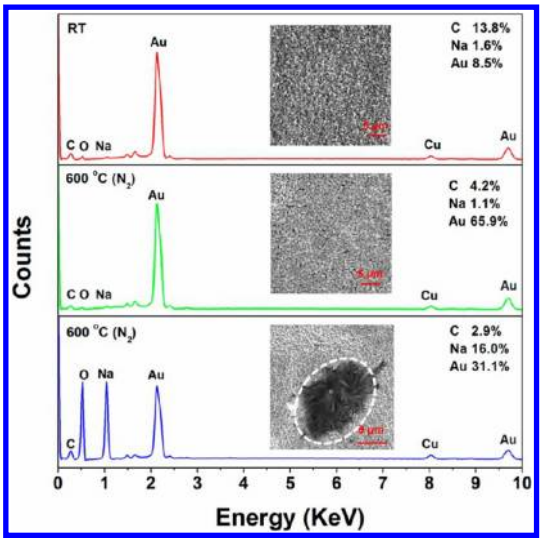

Figure 5. EDX spectra of the sample G/Au = 1:3.1 before (RT) and after two-step annealing treatment with/without the shaded area, respectively.

gold produced by dealloying as reported previously.[35,36] Indeed, we find some imperfect porous structures by SEM with small AuNPs surrounded by large ligaments (Figure S8 in the Supporting Information).

It is notable that recently Chen and Yang's group reported the fabrication of AuNPs embedded porous graphene thin films by layer-by-layer self-assembly and subsequent thermal annealing in air at 340 °C.[30] Similarly, in their work, the thermal annealing treatment was introduced to decompose the capping agent bovine serum albumin (BSA), and they clearly observed the aggregation and size growth of AuNPs. Differing from their work aiming at the application in electrochemical sensing, we adopted a much higher annealing temperature to completely remove the template (graphene sheets).

To further understand the templating effect of graphene sheets on the formation of macroporous structure, we additionally did a control experiment. Other than exposing the graphene/Au hybrid paper in air after thermal annealing in the two-step treatment, we made the hybrid paper cool down still in N_2 atmosphere to retain the template. As shown in Figure 6, if graphene sheets are not removed, no porous structure can be formed as expected, but only irregular large

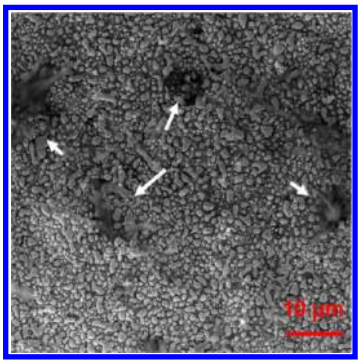

Figure 6. SEM image of the exterior of the sample G/Au = 1:6.3 after thermal annealing and subsequent cooling both in N_2 atmosphere. The white arrows mark the positions of shaded areas.

dx.doi.org/10.1021/am400703v | ACS Appl. Mater. Interfaces 2013, 5, 3481−3486

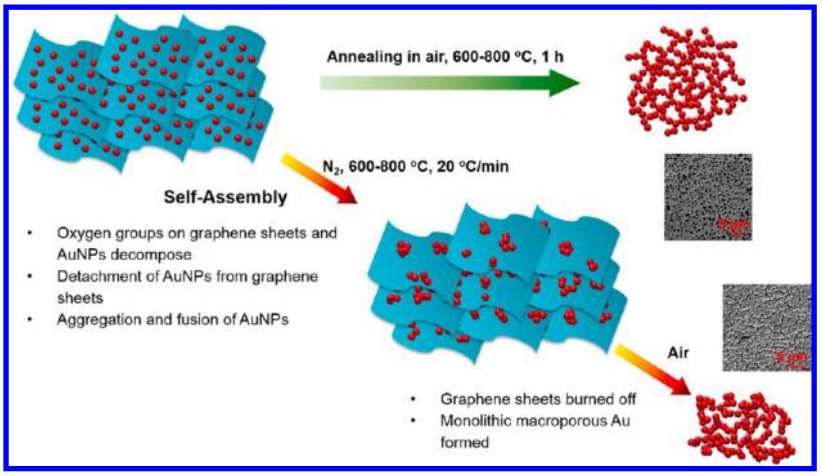

Figure 7. Porosity evolution mechanism of MPG films using graphene sheets as a template upon two thermal annealing procedures.

AuNPs and shaded areas are existing, which also supports our former judgment.

Therefore, we propose the porosity evolution mechanism of MPG films using graphene sheets as a template, as depicted in Figure 7. By direct thermal annealing in air, graphene sheets start to decompose at 600 °C, and only thermally induced aggregation and fusion of AuNPs exist, resulting in a completely interconnected porous structure. Too much or too few AuNPs decorated on graphene sheets both lead to the decrease of porosity. By thermal annealing in N_2 atmosphere, the oxygen groups on graphene sheets and AuNPs start to decompose first causing the detachment of AuNPs from graphene sheets, which subsequently leads to the aggregation and fusion of AuNPs among graphene multilayers into irregular large AuNPs as ligaments. Then exposing the composites in air to remove graphene sheets produces MPG films with different porosity. It is easily accepted that more AuNPs on graphene sheets would lead to the increase of ligament size. Obviously, the two-step treatment has a more significant templating effect than direct thermal annealing to fabricate MPG films, because a preaggregation process of AuNPs assisted by graphene sheets has taken place before the removal of the template.

As reported, porous metals possess outstanding surface plasmon resonance (SPR),[11,37] which have especially gained potenital applications in SERS.[38−40] We also performed Raman experiments to roughly testify the SERS activity of our synthesized MPG films, as shown in Figure 8. NBA was chosen as a model analyte. As expected, the MPG films obtained either by direct thermal annealing or by the two-step treatment show SERS spectra with well-defined high-intensity bands characteristic of NBA: ring stretching (1490, 1435, 1378, and 1320 cm^{-1}) and CH bending (1258 and 1182 cm^{-1}). The MPG film obtained by the two-step treatment exhibits more significant SERS activity than that by direct thermal annealing. It may be caused by the small nanopores and large ligaments in the MPG film obtained by two-step treatment, which, as reported, can produce intensified localized SPR for a high SERS enhancement resulting from strong electromagnetic coupling.[39]

4. CONCLUSION

We have developed a straightforward and environmentally friendly strategy to fabricate MPG films using graphene sheets as a template. Either direct thermal annealing in air or a two-step thermal treatment (in N_2 atmosphere first and subsequently in air) can produce porous nanostructures, but with different morphologies. We further investigated the evolution mechanism of porosity and the effect of graphene/gold weight ratio and annealing temperature on the nanoarchitecture. The two-step treatment was found to show a more significant templating effect than direct thermal annealing to fabricate MPG films due to the existence of a preaggregation process of AuNPs assisted by graphene sheets in N_2. Finally, the resulting MPG films were also found to exhibit excellent SERS activity. Our method can hopefully be extended to the synthesis of other porous materials (such as Ag, Cu, Pt, and ceramic) and much wider applications.

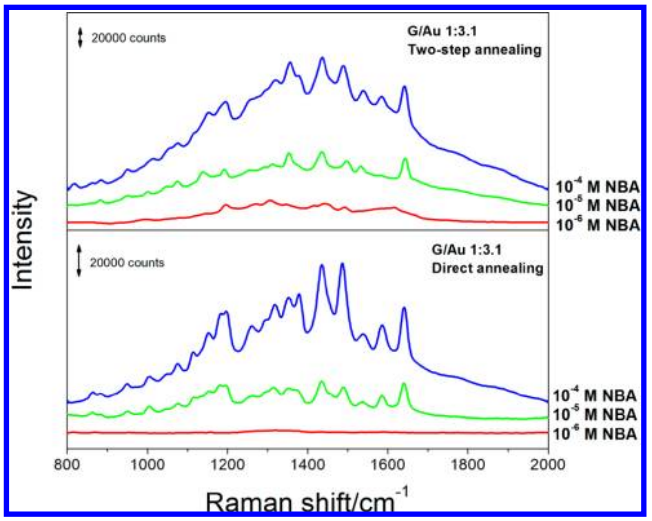

Figure 8. SERS spectra of NBA deposited on MPG films (G/Au = 3.1) upon two thermal annealing procedures (annealing temperature = 600 °C). Raman laser excitation: 785 nm.

■ ASSOCIATED CONTENT

Ⓢ Supporting Information

UV−vis spectra, TEM image, and TGA curves of graphene/AuNPs composites, TGA curves of MPG films, TEM image of the bicontinuous porous structure, pore and ligament size distributions, SEM images of AuNPs films after thermal annealing and the imperfect porous structure in MPG film. This material is available free of charge via the Internet at http://pubs.acs.org.

AUTHOR INFORMATION

Corresponding Author

*E-mail: peiyiwu@fudan.edu.cn.

Notes

The authors declare no competing financial interest.

ACKNOWLEDGMENTS

We gratefully acknowledge the financial support National Science Foundation of China (NSFC) (20934002, 51073043) and the National Basic Research Program of China (No. 2009CB930000).

REFERENCES

(1) Erlebacher, J.; Seshadri, R. *MRS Bull.* **2009**, *34*, 561.
(2) Ding, Y.; Chen, M. *MRS Bull.* **2009**, *34*, 569.
(3) Tappan, B. C.; Steiner, S. A.; Luther, E. P. *Angew. Chem., Int. Ed.* **2010**, *49*, 4544.
(4) Xu, C.; Su, J.; Xu, X.; Liu, P.; Zhao, H.; Tian, F.; Ding, Y. *J. Am. Chem. Soc.* **2007**, *129*, 42.
(5) Asao, N.; Ishikawa, Y.; Hatakeyama, N.; Yamamoto, Y.; Chen, M.; Zhang, W.; Inoue, A. *Angew. Chem., Int. Ed.* **2010**, *49*, 10093.
(6) Wittstock, A.; Zielasek, V.; Biener, J.; Friend, C. M.; Baumer, M. *Science* **2010**, *327*, 319.
(7) Ding, Y.; Chen, M.; Erlebacher, J. *J. Am. Chem. Soc.* **2004**, *126*, 6876.
(8) Yu, C.; Jia, F.; Ai, Z.; Zhang, L. *Chem. Mater.* **2007**, *19*, 6065.
(9) Ding, Y.; Wang, Y.; Su, L. A.; Zhang, H.; Lei, Y. *J. Mater. Chem.* **2010**, *20*, 9918.
(10) Lang, X.; Hirata, A.; Fujita, T.; Chen, M. *Nat. Nanotechnol.* **2011**, *6*, 232.
(11) Biener, J.; Nyce, G. W.; Hodge, A. M.; Biener, M. M.; Hamza, A. V.; Maier, S. A. *Adv. Mater.* **2008**, *20*, 1211.
(12) Shulga, O. V.; Jefferson, K.; Khan, A. R.; D'Souza, V. T.; Liu, J.; Demchenko, A. V.; Stine, K. J. *Chem. Mater.* **2007**, *19*, 3902.
(13) Ciesielski, P. N.; Scott, A. M.; Faulkner, C. J.; Berron, B. J.; Cliffel, D. E.; Jennings, G. K. *ACS Nano* **2008**, *2*, 2465.
(14) Sieradzki, K.; Erlebacher, J.; Karma, A.; Dimitrov, N.; Aziz, M. *Nature* **2001**, *410*, 450.
(15) Snyder, J.; Asanithi, P.; Dalton, A. B.; Erlebacher, J. *Adv. Mater.* **2008**, *20*, 4883.
(16) Erri, P.; Nader, J.; Varma, A. *Adv. Mater.* **2008**, *20*, 1243.
(17) Walsh, D.; Arcelli, L.; Ikoma, T.; Tanaka, J.; Mann, S. *Nat. Mater.* **2003**, *2*, 386.
(18) Nyce, G. W.; Hayes, J. R.; Hamza, A. V.; Satcher, J. H. *Chem. Mater.* **2007**, *19*, 344.
(19) Hong, G. S.; Li, C.; Qi, L. M. *Adv. Funct. Mater.* **2010**, *20*, 3774.
(20) Yang, Q.; Liang, S. H.; Han, B. B.; Wang, J.; Mao, R. *Mater. Lett.* **2012**, *73*, 136.
(21) Fang, C.; Bandaru, N. M.; Ellis, A. V.; Voelcker, N. H. *J. Mater. Chem.* **2012**, *22*, 2952.
(22) He, H.; Cai, W. P.; Lin, Y. X.; Chen, B. S. *Chem. Commun.* **2010**, *46*, 7223.
(23) Bai, H.; Li, C.; Shi, G. *Adv. Mater.* **2011**, *23*, 1089.
(24) Guo, S.; Dong, S. *Chem. Soc. Rev.* **2011**, *40*, 2644.
(25) Goncalves, G.; Marques, P. A. A. P.; Granadeiro, C. M.; Nogueira, H. I. S.; Singh, M.; Gracio, J. *Chem. Mater.* **2009**, *21*, 4796.
(26) Zhang, Z.; Xu, F.; Yang, W.; Guo, M.; Wang, X.; Zhang, B.; Tang, J. *Chem. Commun.* **2011**, *47*, 6440.
(27) Lu, G.; Li, H.; Liusman, C.; Yin, Z.; Wu, S.; Zhang, H. *Chem. Sci.* **2011**, *2*, 1817.
(28) Huang, J.; Zhang, L.; Chen, B.; Ji, N.; Chen, F.; Zhang, Y.; Zhang, Z. *Nanoscale* **2010**, *2*, 2733.
(29) Xiang, J.; Drzal, L. T. *ACS Appl. Mater. Interfaces* **2011**, *3*, 1325.
(30) Xi, Q.; Chen, X.; Evans, D. G.; Yang, W. S. *Langmuir* **2012**, *28*, 9885.
(31) Hummers, W. S.; Offeman, R. E. *J. Am. Chem. Soc.* **1958**, *80*, 1339.
(32) Sun, S.; Wu, P. *Phys. Chem. Chem. Phys.* **2011**, *13*, 21116.
(33) Zhang, Z.; Chen, H.; Xing, C.; Guo, M.; Xu, F.; Wang, X.; Gruber, H. J.; Zhang, B.; Tang, J. *Nano Res.* **2011**, *4*, 599.
(34) Bagri, A.; Mattevi, C.; Acik, M.; Chabal, Y. J.; Chhowalla, M.; Shenoy, V. B. *Nat. Chem.* **2010**, *2*, 581.
(35) Hakamada, M.; Mabuchi, M. *J. Mater. Res.* **2009**, *24*, 302.
(36) Tan, Y. H.; Davis, J. A.; Fujikawa, K.; Ganesh, N. V.; Demchenko, A. V.; Stine, K. J. *J. Mater. Chem.* **2012**, *22*, 6733.
(37) Yu, F.; Ahl, S.; Caminade, A. M.; Majoral, J. P.; Knoll, W.; Erlebacher, J. *Anal. Chem.* **2006**, *78*, 7346.
(38) Kucheyev, S.; Hayes, J.; Biener, J.; Huser, T.; Talley, C.; Hamza, A. *Appl. Phys. Lett.* **2006**, *89*, 053102.
(39) Lang, X.; Chen, L.; Guan, P.; Fujita, T.; Chen, M. *Appl. Phys. Lett.* **2009**, *94*, 213109.
(40) Zhang, L.; Lang, X.; Hirata, A.; Chen, M. *ACS Nano* **2011**, *5*, 4407.